Pergamon

*Solid-State Electronics* Vol. 41, No. 8, pp. 1139–1152, 1997

Printed in Great Britain
PII: S0038-1101(97)00051-8
0038-1101/97 $17.00 + 0.00

# PHYSICAL MODELS FOR STRAINED AND RELAXED GaInAs ALLOYS: BAND STRUCTURE AND LOW-FIELD TRANSPORT

Ch. KÖPF, H. KOSINA and S. SELBERHERR
Institute for Microelectronics, TU Vienna, Gusshausstrasse 27–29, A-1040 Vienna, Austria

*(Received 9 July 1996; in revised form 14 January 1997)*

**Abstract**—We describe models for physical properties of the technologically significant GaInAs material system with respect to its composition and strain conditions introduced by strained-layer heteroepitaxy. We give an empirical relation for the critical thickness which takes growth conditions into account and allows the residual strain for layer thicknesses exceeding the critical one to be estimated. Easy to use models for the band edge energy and effective mass are presented, which are based on deformation potential and $\mathbf{k}\cdot\mathbf{p}$ theory. Monte Carlo calculations were employed to obtain a model for the anisotropic electron mobility. All models are given as functions of the independent parameters composition and strain which are no longer strictly coupled in the relaxed case.

## 1. INTRODUCTION

The properties of electronic devices are often tailored by forming heterostructures of either the group IV or III–V alloys. Modern growth techniques give excellent material control and interface quality. Special optical and electronic properties can be obtained by proper alloying of semiconductors. The introduction of elastic strain through heteroepitaxy of lattice-mismatched materials gives an additional degree of freedom and thus greatly enhances the variability of obtaining desired material characteristics.

We investigate basic properties and low-field transport of the important GaInAs system in view of strain effects and give formulations suited for device simulation. The organization of this article is as follows. First the effects of alloying and strain on the bulk band structure are sketched. An estimation of the elastic strain for partially relaxed layers is outlined. Then the dependence of the band edge energies and effective masses on temperature and strain is given. Finally the electron mobility is investigated on the basis of Monte Carlo simulation. Easy to use models for the above quantities are constructed.

## 2. BASIC PROPERTIES OF BULK ALLOYS

The materials under consideration consist of the binaries GaAs and InAs, which because of their zinc-blende crystal structure show the same symmetry. The electronic properties are governed by the band structure, which is described by the ellipsoidal many-valley model consisting of a single spherical valley at $\Gamma$ [000], four energy degenerate valleys at the $L$ point $\langle 111\rangle$ and six valleys along the $\Delta$ lines $\langle 100\rangle$ very close to the $X$ point. Therefore we call the latter $X$ valleys in the sequel. The validity range of the parabolic dispersion in energy can be extended by introducing a nonparabolicity parameter $\alpha$. The valence band consists of the degenerate heavy and light hole bands (hh, lh) and the split-off band (so). Formulations like the warped-band model or more elaborate descriptions like spherical harmonics representation[1] must be used for higher energy.

When alloys are formed, the lattice structure of the basic binaries is retained. The probability of finding a specific cation or anion species at a certain lattice site is assumed to be proportional to the composition ratio of the species. This random alloy approximation is used in the sequel; clustering and superlattices are not considered.

### 2.1. *Interpolation*

In view of the multitude of semiconductor alloys, it is clear that not all physical properties necessary for device and research purposes were evaluated from experiment. In addition, some physical quantities of alloys are hard to derive from first principles. Band structure calculations, for example, are complicated enormously by the fact that a random alloy is not crystalline in a strict sense, such that Bloch wave functions cannot be used to describe electron states. Therefore it is necessary to estimate quantities from the values of the constituting basic materials. This can be done by interpolation as described in the following.

According to Vegard's law, the physical parameters of ternary alloys $\mathscr{T}$ can be interpolated linearly from the corresponding binaries' quantities $\mathscr{B}$

caused by the similarity of the alloy and its constituents;

$$\mathscr{T}(x) = x\mathscr{B}_1 + (1-x)\mathscr{B}_2. \quad (1)$$

However, some properties exhibit a nonlinear dependence on the composition $x$. Typical examples are the band edge energies. In random alloys the symmetry of the band structure remains unchanged, however, the nonlinearity is caused by the disorder of the perfect crystal lattice[2]. The band edge energies can be approximated by a quadratic function using the so-called bowing factor $C$;

$$\mathscr{T}(x) = x\mathscr{B}_1 + (1-x)\mathscr{B}_2 - x(1-x)C_{12}. \quad (2)$$

Some physical quantities require higher-order polynomials for accurate description. In Table 1 numerical values for band quantities are given. The parameters for the higher minima of InAs are not well characterized, so we quote both mostly given values for the $L$ and $X$ gaps. The conduction band bowing factors are obtained by matching data at intermediate indium compositions (especially the InP lattice-matched $Ga_{0.47}In_{0.53}As$), the bowing of the split-off band is estimated following Adachi[3].

## 3. LATTICE MISMATCH STRAIN

Within this section the effects of strain which result from lattice-mismatched epitaxy are considered. A change of the crystal symmetry and hence the band structure can be observed. Strained-layer epitaxy produces biaxial stress parallel to the interface; in the perpendicular direction no stress is built up. The interdependence of stress and strain is assumed to remain completely in the linear range of Hooke's law.

The components of the strain tensor are functions of the interface orientation[4] and the lattice misfit. For an epilayer with lattice constant $a$ on a thick substrate with lattice constant $a_{sub}$ the misfit is defined as;

$$f_0 = \frac{a - a_{sub}}{a_{sub}}. \quad (3)$$

Under the assumption of coherent growth, the in-plane strain in the epilayer and the perpendicular component are;

$$e_\parallel = \frac{a_{sub} - a}{a} \quad e_\perp = -\frac{e_\parallel}{\sigma}. \quad (4)$$

Here $\sigma$ denotes the Poisson ratio for the biaxial strain condition which depends on the elastic constants $c_{ij}$ and the interface orientation[5]. Since $a \approx a_{sub}$ it holds $e_\parallel \approx -f_0$. For the most important (001) orientation the shear components of the strain tensor vanish;

$$e_{xx} = e_{yy} = e_\parallel \quad e_{zz} = -\frac{2c_{12}}{c_{11}} e_\parallel, \quad (5)$$

$$e_{xy} = e_{yz} = e_{zx} = 0.$$

For (111) interfaces follows;

$$e_{xx} = e_{yy} = e_{zz} = \frac{4c_{44}}{c_{11} + 2c_{12} + 4c_{44}} e_\parallel, \quad (6)$$

$$e_{xy} = e_{yz} = e_{zx} = \frac{2c_{11} + 4c_{12}}{c_{11} + 2c_{12} + 4c_{44}} e_\parallel.$$

### 3.1. Strain relaxation

If the thickness of an epitaxy layer exceeds a certain critical thickness $h_c$, strain relaxation occurs. The determination of this value and the strain state is important both for intentionally pseudomorphic (channel of HFETs) and relaxed (buffer) layers. The main effect which reduces the strain in the epilayer is dislocation generation. Other effects are islanding, i.e. three-dimensional growth, or segregation of alloy components. The calculation of the critical thickness for dislocation free growth was addressed by Frank and Van der Merwe first, yielding an approximate hyperbolic dependence $h_c \propto b/f_0$, valid for low misfit. The widely used model of Matthews and Blakeslee (MB)[6–8], which relies on equilibrium force balance at the interface, gives;

$$h_c = \frac{b(1 - \nu\cos^2\theta)}{4\pi f_0(1+\nu)\sin\theta\cos\lambda} \ln\left(\alpha\frac{h_c}{b}\right) \quad (7)$$

where $b = a/\sqrt{2}$ is Burger's vector, $\theta$ and $\lambda$ give the

Table 1. Band parameters—temperature dependence (300 K values if not explicitly defined)

| Quantity | GaAs | | | InAs | | | Unit |
|---|---|---|---|---|---|---|---|
| | $\Gamma$ | $L$ | $X$ | $\Gamma$ | $L$ | $X$ | |
| $E$ | 1.424[n] | 1.734[o] | 1.911[o] | 0.356[q] | 1.07[r], 1.434[s] | 1.37[r], 1.963[s] | eV |
| $E$(0 K) | 1.517[t] | 1.815[p] | 1.981[p] | 0.42[t] | | | eV |
| $dE/dT$ | −3.95[r] | −5.06[a] | −3.85[a] | −3.5[r] | | | $10^{-4}$ eV/K |
| $A$ | 5.5[t] | 6.05[p] | 4.6[p] | 2.76[t] | | | $10^{-4}$ eV/K |
| $B$ | 225.0[t] | 204.0[p] | 204.0[p] | 83.0[t] | | | K |
| $m$(0 K) | 0.067[a] | | | 0.0236[t] | | | $m_0$ |
| $m_l$ | 0.063[a] | 1.9[g] | 1.3[a] | | 1.565[s] | 3.619[s] | $m_0$ |
| $m_t$ | 0.063 | 0.0754[a] | 0.23[a] | | 0.124[s] | 0.271[s] | $m_0$ |
| $C_\Gamma$ | | | | 0.45 | | | eV |
| $C_L$ | | | | 0.33[t],1.10[u] | | | eV |
| $C_X$ | | | | 0.75[t],2.0[u] | | | eV |
| $C_{\Delta 0}$ | | | | 0.178 | | | eV |

[a] Ref. [56]; [r] Ref. [57]; [g] Ref. [58]; [t] Ref. [59]; [t] Ref. [60]; [n] Ref. [56]; [o] Ref. [61], [62]; [p] Ref. [58], $B$ assumed equal to $\Gamma$ value; [q] Ref. [63]; [r] Ref. [3], Ref. [64]; [s] Ref. [52], loc.emp.pseudopot.calc; [t] calc. using $E^{L,X}_{InAs}$ of Ref. [3]; [u] calc. using $E^{L,X}_{InAs}$ of Ref. [52].

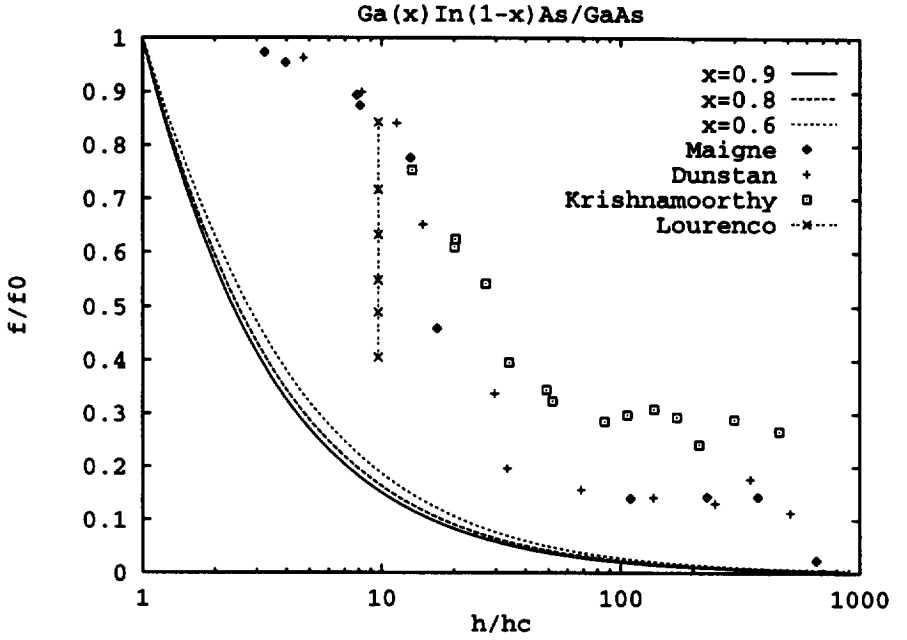


Fig. 1. Relative residual strain $f/f_0$ vs normalized layer thickness $h/h_c$ after the MB model.

orientation of the dislocation lines, and $\alpha$ is the dislocation "core" parameter (originally given as "e") which is usually fitted to experiment in the range 1–4[9,10]. For edge dislocations, $\theta = \pi/2$, $\lambda = 0$, while for 60° dislocations $\theta = \lambda = \pi/3$. For (001) interfaces at low misfit ($f_0 < 2\%$), 60° dislocations predominate, while for high strain the edge type is favored which is more efficient in relieving strain energy and has lower $h_c$[11].

Equation (7) allows us in turn to calculate the residual strain $f$ if the thickness exceeds $h_c$. In Fig. 1 the residual strain normalized to the fully coherent strain vs the epilayer thickness normalized to $h_c$ (MB) is compared with various studies of as-grown samples[12–14] and thermally annealed ones[15]. The predicted relative residual strain is independent of composition as is observed by experiment. The large discrepancy obviously supports the observation of coherent growth far beyond the critical thickness of MB. To deal with that fact the inclusion of friction into the force balance was proposed. However, incorporating Peierl's stress, which is the most important one, does not give satisfactory improvement either, though it enhances $h_c$ and introduces the growth temperature as a parameter[16]. A model based on energy balance at the interface was proposed by People and Bean[17,18]. Originally given for edge dislocations in SiGe/Si, it also predicts higher $h_c$ especially at low strains. The comparison with the measured data in the case of GaInAs/GaAs is still not satisfying. In addition, growth conditions are also not included explicitly.

The experimental values show clearly that growth conditions and subsequent thermal treatment (annealing) have a large influence on the residual strain. Very high annealing temperatures and/or times are needed to attain the values of the MB model[19]. Since we are interested in estimating the remaining steady-state strain, we propose a simple empirical relation for the residual strain including both growth and annealing temperatures $T_g$, $T_a$. The critical thickness we model by;

$$h_c(T_g) = \frac{h_0(T_g)}{(f_0 \cdot (1 - f_{min}(T_g)))^{\zeta}}. \tag{8}$$

The resulting relative strain (as-grown) is;

$$\frac{f}{f_0}(h, T_g) = \frac{1}{f_0} \cdot \left(\frac{h_0(T_g)}{h}\right)^{1/\zeta} + f_{min}(T_g). \tag{9}$$

Annealing at $T_a$ reduces $f$ further to;

$$\frac{f_{ann}}{f_0}(h, T_g, T_a) = \frac{f}{f_0}(h, T_g) - f_a(T_a, T_g). \tag{10}$$

Expressions for the fit parameters can be found in Table 2. The Ansatz relies on the observation that $f/f_0$ is independent of composition at very large thicknesses, i.e. $h_0$ and $f_{min}$ only depend on growth

Table 2. Model parameters for the empirical critical thickness and residual strain model

| | |
|---|---|
| $h_0$ (nm) | $0.73 - 0.0011 \cdot \left(\frac{T_g}{°C} - 520\right)$ |
| $f_{min}$ | $0.09 - 7.62 \times 10^{-3} \cdot \left(\frac{T_g}{°C} - 520\right) + 2.721 \times 10^{-6} \cdot \left(\frac{T_g}{°C} - 520\right)^2$ |
| $f_a$ | $1.95 \times 10^{-6} \cdot \left(\frac{T_a - T_g}{°C}\right)^2$ |
| $\zeta$ | 1.0 |

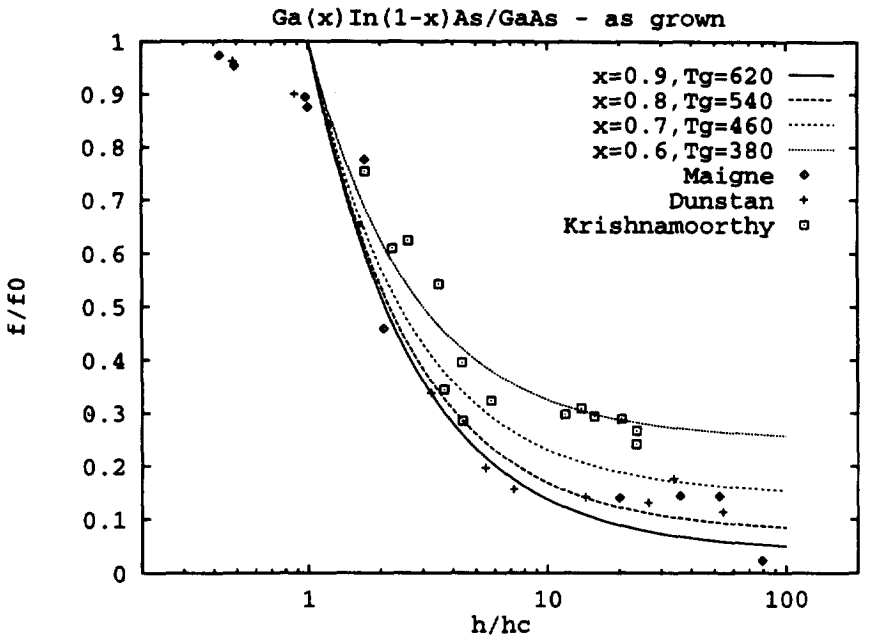


Fig. 2. Relative residual strain $f/f_0$ vs normalized layer thickness $h/h_c$ (empirical model, as-grown).

temperature. In Fig. 2 the measurements[12–14] are shown in comparison with the empirical model (9). The correspondence is good, except at the onset of relaxation ($h \lesssim h_c$). In Fig. 3 the annealing experiment of [15] is compared with (10). We note that annealing near the melting point would be required to attain the MB strain.

Bearing in mind the complicated thermally activated transient process of conversion from elastic to plastic strain, the proposed relations should only be a guideline for estimating the residual strain in the low to moderate strain (composition) range at the usual growth temperatures. An important point is that layers grown beyond the equilibrium $h_c$ are metastable in principle, but their metastability is very robust. The (as-grown) model will be applicable in most cases and the MB model can be considered a limiting case.

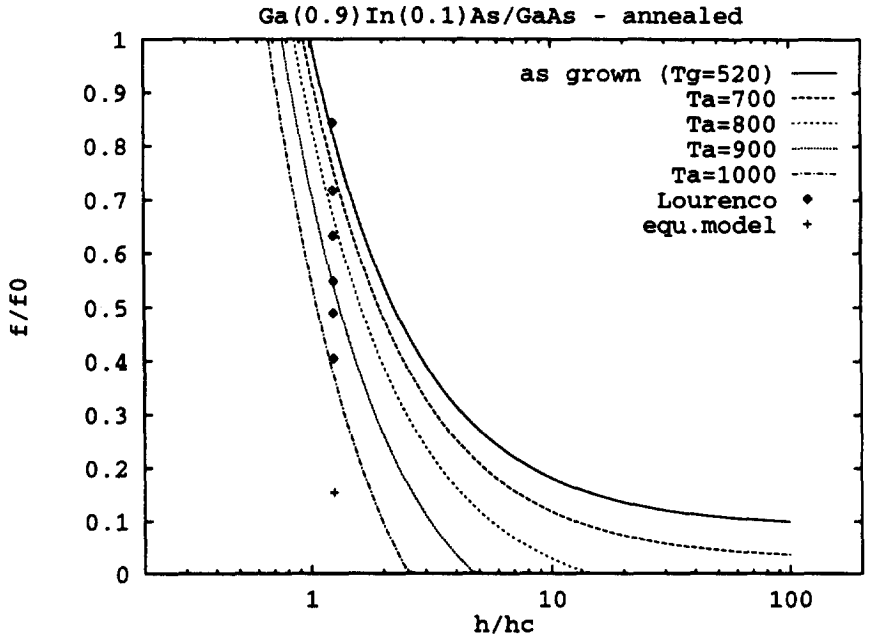


Fig. 3. Relative residual strain $f/f_0$ vs normalized layer thickness $h/h_c$ (empirical model, annealed).

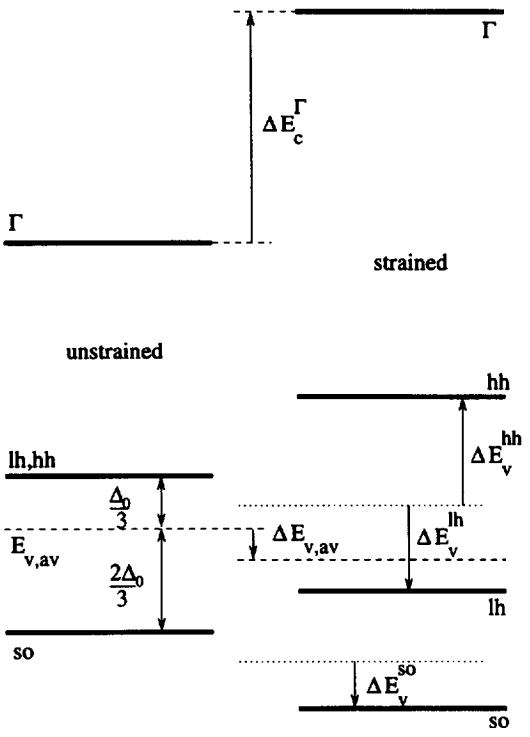


Fig. 4. Band edges for unstrained and (compressively) strained III–V semiconductors.

## 4. BAND EDGES

### 4.1. Temperature effects

The characteristic thermal behavior of the band gaps is usually described by Varshni's equation[20];

$$E^i(T) = E^i(0) - \frac{A^i T^2}{T + B^i}, \tag{11}$$

which is similar to a parabolic dependence at low $T$, changing into linearity at high $T$. In Table 1 numerical values are given. Since parameters for the higher minima of InAs are not well characterized, we assume the same $T$ dependence as for the direct gap.

### 4.2. Strain effects

Strain effects on the band edge energies can be described following the deformation potential theory of Brooks[21], Herring and Vogt[22], and Kane[23]. The shift of band edges can be decomposed into a term, further called hydrostatic, affecting the average of a certain degenerate conduction band minimum or the valence band and a term, called uniaxial, influencing each individual minimum (Fig. 4). To simplify and unify the notation we use $A_i^j$ and $B_i^j$ for the hydrostatic and uniaxial deformation potentials, respectively, both for conduction and valence band (index $i$) with appropriate superscript $j$ denoting either valley (conduction band) or interface strain orientation (valence band).

*4.2.1. Hydrostatic contributions.* One must distinguish clearly between changes of band energy differences, i.e. gaps and changes of the band edges on an absolute scale. The latter are very difficult to obtain from measurements, whereas changes of band gaps are readily obtained from pressure experiments. The hydrostatic term is related to volume changes of the crystal which can be expressed by the strain tensor $\mathbf{e}$;

$$\frac{\Delta V}{V} = Tr(\mathbf{e}) = e_{xx} + e_{yy} + e_{zz}. \tag{12}$$

The average shift of either a conduction or valence band is described by the hydrostatic or dilatation deformation potentials $A_v$ and $A_c^i$ ($i = \Gamma, L, X$);

$$\Delta E_{v,av} = A_v Tr(\mathbf{e}) \quad \Delta E_{c,av}^i = A_c^i Tr(\mathbf{e}). \tag{13}$$

For the direct $\Gamma$ valley this is already the complete strain dependence. The band gap deformation potentials $A^i$ which are mostly tabulated are of course $A^i = A_c^i - A_v$. Via the bulk modulus $B$, they are connected to the pressure coefficient of the band gaps. Since $dV/dp = -V/B$ and for cubic crystals $B = \frac{1}{3}(c_{11} + 2c_{12})$, it holds;

$$A^i = -\frac{1}{3}(c_{11} + 2c_{12})\frac{dE^i}{dp}. \tag{14}$$

*4.2.2. Uniaxial conduction band splittings.* The uniaxial contributions partially lift the energy degeneracy of the indirect conduction band minima. For a (001) interface, the splittings of the individual $X$ valleys with respect to the average are given by;

$$\Delta E_c^{001} = -\frac{2}{3} B_c^X (e_{xx} - e_{zz}) \tag{15}$$

$$\Delta E_c^{010} = \Delta E_c^{100} = \frac{1}{3} B_c^X (e_{xx} - e_{zz}).$$

The $L$ valleys are not affected by this kind of strain;

$$\Delta E_c^{111} = \Delta E_c^{\bar{1}11} = \Delta E_c^{1\bar{1}1} = \Delta E_c^{11\bar{1}} = 0. \tag{16}$$

For (111) interfaces the situation is reverted. The $X$ valleys remain degenerate;

$$\Delta E_c^{001} = \Delta E_c^{010} = \Delta E_c^{100} = 0, \tag{17}$$

and the $L$ valleys are split;

$$\Delta E_c^{111} = 2B_c^L e_{xy} \tag{18}$$

$$\Delta E_c^{\bar{1}11} = \Delta E_c^{1\bar{1}1} = \Delta E_c^{11\bar{1}} = -\frac{2}{3} B_c^L e_{xy}.$$

*4.2.3. Uniaxial valence band splittings.* The strain effect on the valence band was investigated by Kleiner and Roth[24], Pollak and Cardona[25], and Bir and Pikus[26]. In the unstrained case, spin-orbit coupling leads to a twofold degenerate pair commonly termed light and heavy hole bands at $E_{v,av} + \frac{1}{3}\Delta_0$ and the split-off band below the average $E_{v,av} - \frac{2}{3}\Delta_0$. $\Delta_0$ is the spin-orbit energy. Uniaxial strain components lift the degeneracy of the lh and hh states. The individual

Table 3. Measured bulk parameters and deformation potentials

| Quantity | GaAs | | | InAs | | | Unit |
|---|---|---|---|---|---|---|---|
| $a$ | 5.653[f] | | | 6.058[f] | | | Å |
| $c_{11}$ | 11.88[b] | | | 8.329[b] | | | $10^{10}$Pa |
| $c_{12}$ | 5.38[b] | | | 4.526[b] | | | |
| $c_{44}$ | 5.94[b] | | | 3.959[b] | | | |
| $E_p$ | 22.5[l], 25.7[r] | | | 20.56[l], 22.2[hu] | | | eV |
| $\Delta_0$ | 0.34[b] | | | 0.38[h] | | | eV |
| $A_v$ | −0.7[r] | | | | | | eV |
| $B_v^{001}$ | −1.7[b], −2.0[a] | | | −1.8[b] | | | eV |
| $B_v^{111}$ | −4.55[b] | | | −3.6[b] | | | eV |
| | Γ | $L$ | $X$ | Γ | $L$ | $X$ | |
| $dE/dp$ | 10.73[m] | 2.8[mo] | −1.34[m], −0.8[o] | 10.0[m],11.4[l] | 4.0[p] | −2.1[p] | $10^{-11}$ eV/Pa |
| $A_c$ | −9.3[r], −8.6[s], −7.0[x] | −2.8[x] | 0.3[x] | −5.8[x] | | | eV |
| $B_c$ | — | 19.6[a] | — | | −3.6[a] | | eV |
| $A$ | −9.77[a], −8.1[y] | −2.1[y] | 1.01[y] | −6.0[a], −5.8[y] | −2.32[y] | 1.22[y] | eV |

[a] Ref. [65]; [b] Ref. [57]; [r] Ref. [66]; [h] Ref. [47]; [i] Ref. [67]; [l] Ref. [59]; [m] Ref. [60]; [o] Ref. [68]; [p] Ref. [64]; [r] Ref. [69]; [s] Ref. [70]; [v] Ref. [27]; [x] calc. from $A$ and $A_v$; [y] calc. from eqn (14).

Table 4. Calculated band parameters and deformation potentials (after Ref. [28])

| Quantity | GaAs | | | InAs | | | Unit |
|---|---|---|---|---|---|---|---|
| $E_{v,av}$ | −6.92 | | | −6.67 | | | eV |
| $A_v$ | 1.16, −1.6[a] | | | 1.0, −0.6[a] | | | eV |
| $B_v^{001}$ | −1.9 | | | −1.55 | | | eV |
| $B_v^{111}$ | −4.23 | | | −3.1 | | | eV |
| | Γ | $L$ | $X$ | Γ | $L$ | $X$ | |
| $A_c$ | −7.17, −8.8[a] | −4.4[a] | 0.5[a] | −5.08, −7.3[a] | −3.0[a] | 1.3[a] | eV |
| $B_c$ | — | 14.26 | 8.61 | — | 11.35 | 4.5 | eV |
| $A$ | −8.33, −7.2[a] | −2.8[a] | 2.1[a] | −6.08, −6.7[a] | −2.4[a] | 1.9[a] | eV |

[a] Ref. [27].

uniaxial shifts can be expressed as[25];

$$\Delta E_v^{hh} = -\delta E \tag{19}$$

$$\Delta E_v^{lh} = \frac{1}{2}(-\Delta_0 + \delta E + \sqrt{\Delta_0^2 + 2\Delta_0\delta E + 9\delta E^2})$$

$$\Delta E_v^{so} = \frac{1}{2}(+\Delta_0 + \delta E - \sqrt{\Delta_0^2 + 2\Delta_0\delta E + 9\delta E^2})$$

where for (001) respectively (111) strain condition;

$$\delta E = -B_v^{001}(e_{xx} - e_{zz}) \quad \delta E = \sqrt{3}B_v^{111}e_{xy}. \tag{20}$$

For any other orientation no closed-form expression can be given.†

*4.2.4. Total shift.* The total shifts of the band edges on an absolute scale for the conduction band ($j$ denotes any minimum in valley $i$) and valence band ($j$ is any of hh, lh, so) are;

$$\Delta E_c^i = \Delta E_{c,av}^i + \min_j (\Delta E_c^j) \tag{21}$$

$$\Delta E_v = \Delta E_{v,av} + \max_j (\Delta E_v^j).$$

The band gap shifts are of course $\Delta E^i = \Delta E_c^i - \Delta E_v$.

In Table 3 measured values for the strain parameters are given. Since experimental results for the deformation potentials are either missing (especially for the upper valleys of InAs) or show substantial scatter, calculated values are required. In Table 4 we summarize calculated parameters by Cardona and Christensen[27] and Van de Walle[28]. We prefer the latter, since they are more consistent with measurement and the pressure derivative, which is a useful test. Though the numerical values of $A_c$ and $A_v$ differ, the hydrostatic effect on the Γ valley is much larger than on the valence band (at least by a factor 5). The higher valleys are affected less; the $X$ valley shift even has opposite sign.

The total absolute shifts can be approximated by a polynomial in $e_\parallel$ with material dependent coefficients;

$$\Delta E^i = \sum_{m=1}^{3}\sum_{n=0}^{2} p_{mn}^i x^n e_\parallel^m. \tag{22}$$

The shifts of the conduction band minima and hh band are linear in strain, for the lh and so band higher order terms are required. The coefficients $p_{mn}$ of the interpolating polynomial are given in Table 5. The degree of the $x$ polynomial was chosen in order to keep the relative error below 1%.

Figure 5 depicts the room temperature direct gap of $Ga_xIn_{1-x}As$ vs strain for different compositions. The band gap range which can be reached by coherent (001) growth in the GaAs-InAs system is indicated by the boundaries for GaAs and InAs substrate. Besides the important Ga-rich alloys on GaAs substrate, the nearly InP-matched alloys are well characterized. Both compressive and tensile strain can be studied in the latter case. However, large-strain materials recently became important research topics. InAs-strained systems gain importance, especially for high-speed low-$T$ applications.

In Figure 6 the strain dependent shift of the direct gap is shown for $Ga_xIn_{1-x}As$ on InP. Biaxial compression ($x < 0.47$, $e < 0$) increases the gap at a smaller slope than in-plane tension ($x > 0.47$, $e_\parallel > 0$) decreases it. Agreement of (22) with measurements both at 300 K[29] and low temperature[30,31] and the

†The deformation potentials $A_v$, $B_v^{001}$, and $B_v^{111}$ are usually given in the Bir and Pikus notation as $a$, $b$, and $d$, respectively.

Table 5. Polynomial coefficients for band edge shifts under (001) strain

| | $p_{10}$ | $p_{11}$ | $p_{12}$ | $p_{20}$ | $p_{21}$ | $p_{22}$ | $p_{30}$ | $p_{31}$ | $p_{32}$ |
|---|---|---|---|---|---|---|---|---|---|
| $\Delta E_c^{\Gamma}$ | −4.64 | −3.21 | | | | | | | |
| $\Delta E_c^{\Gamma[111],\Gamma[\bar{1}\bar{1}\bar{1}]}$ | −2.74 | −2.08 | | | | | | | |
| $\Delta E_c^{X[001]}$ | −5.08 | −5.32 | | | | | | | |
| $\Delta E_c^{X[010],X[100]}$ | 4.32 | 2.00 | −0.31 | | | | | | |
| $\Delta E_v^{hh}$ | −2.31 | −0.033 | | | | | | | |
| $\Delta E_v^{lh}$ | 4.15 | 0.74 | | 55.07 | 17.00 | 5.04 | −469.5 | −231.8 | −119.2 |
| $\Delta E_v^{so}$ | 0.92 | 0.355 | | −55.07 | −17.00 | −5.04 | 469.5 | 231.8 | 119.2 |

tight-binding calculations[32] is good. The 300 K linear fit[33] predicts a larger shift for In-rich material. An important conclusion we can draw is that the strain shifts are almost independent of temperature as also pointed out in [34], though most basic parameters used are room temperature values. Figure 7 depicts the room temperature gap under various strain conditions. Also shown are the experimental fits of Bassignana *et al.*[31], who obtained a linear $x$ dependence of the gap, and Singh[33] giving a linear dependence of the gap shift at low strains. The data of Taguchi and Ohno[35] are self-consistent pseudopotential calculations.

### 4.3. Combination

In principle one could calculate any band edge or gap energy from (11, 13, 15–20) and the strain tensor in a straightforward manner by interpolating all basic parameters using the described formulas. However, we prefer a different approach. First, we calculate the temperature dependent band edges of the binaries $E_j^i(T)$, and interpolate over material composition[36]. Finally we add the strain effects. The fundamental band gap can therefore be expressed as;

$$E_g(x, T, e_\parallel) = \min_i (E^i(\Delta E^i(x, e_\parallel), E^i(x, E_1^i(T), E_2^i(T)))). \quad (23)$$

### 4.4. A note on band offsets

The formulation of the band edge shifts on an absolute scale allows to calculate band offsets also at strained heterojunctions virtually as the differences of the respective band edges of the neighboring materials. Common to all such general purpose or linear theories is the connection to a general fixed energy reference level from which valence band edges and hence differences at heterojunctions are inferred. From the very first electron affinity rule of Anderson[37], a variety of such universal references was proposed, the most prominent by Harrison[38,39], Van Vechten[40], Tersoff[41], and Van de Walle and Martin[28,42]. A comprehensive overview can be found in [43,44]. The most intriguing

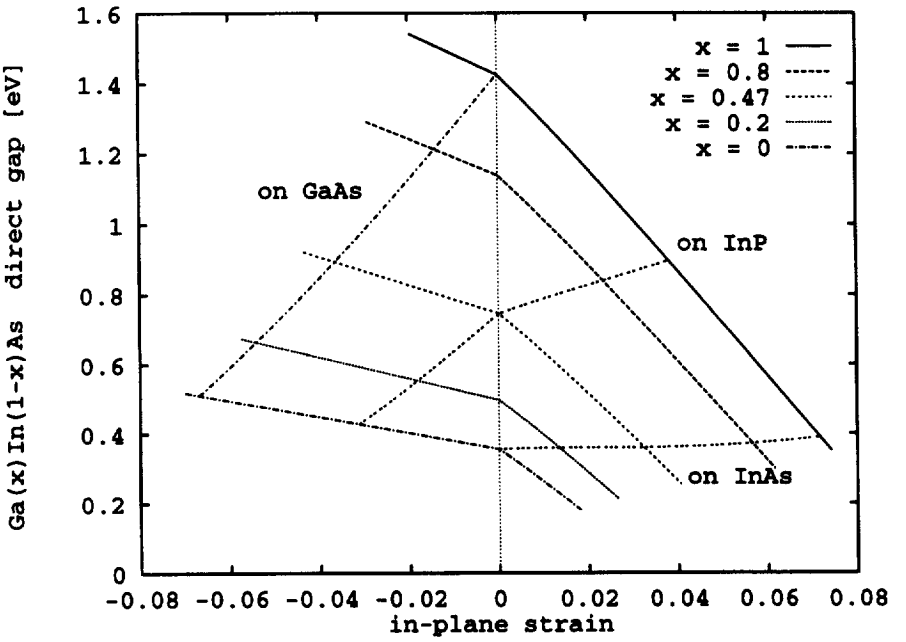


Fig. 5. Direct gap $E^{\Gamma}$ in the GaAs-InAs system versus $e_\parallel$ at 300 K.

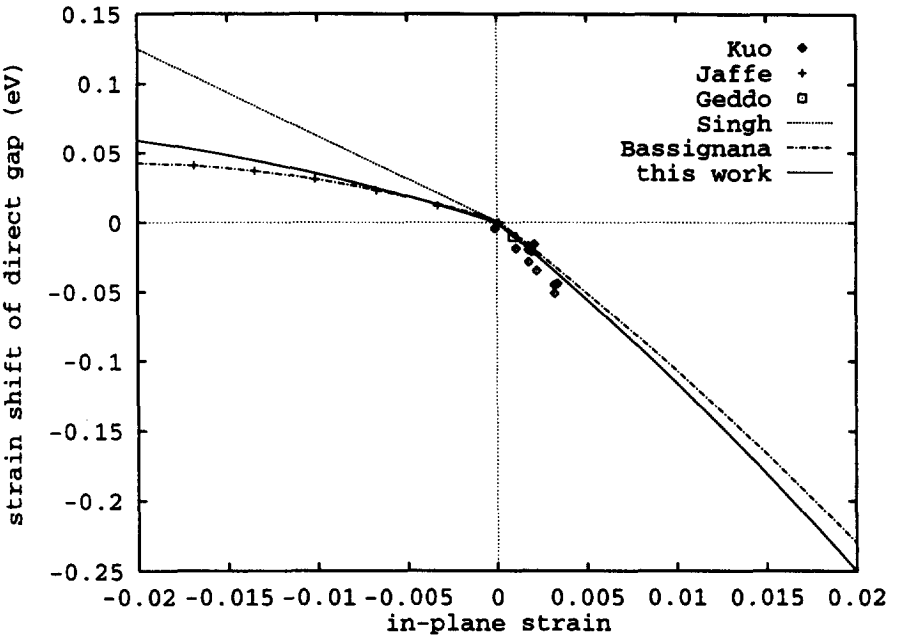


Fig. 6. Shift of direct gap ($E^{\Gamma}_{str}(x) - E^{\Gamma}(x)$) for $Ga_xIn_{1-x}As$ coherently strained on InP (001) substrate vs $e_{\perp}$.

features are commutativity and transitivity which allow to relate all the band edges within a heterojunction device to a single reference of arbitrary choice. However, the various approaches lack the influences of the microscopic conditions at the interface.

A critical point seems to be the detailed atomic arrangement at the interface, i.e. the layer separation at the interface which may be changed by strain conditions. Via the change of the microscopic charge distribution, strain affects the alignment similar to dipole effects. Oloumi and Matthai[45] have obtained

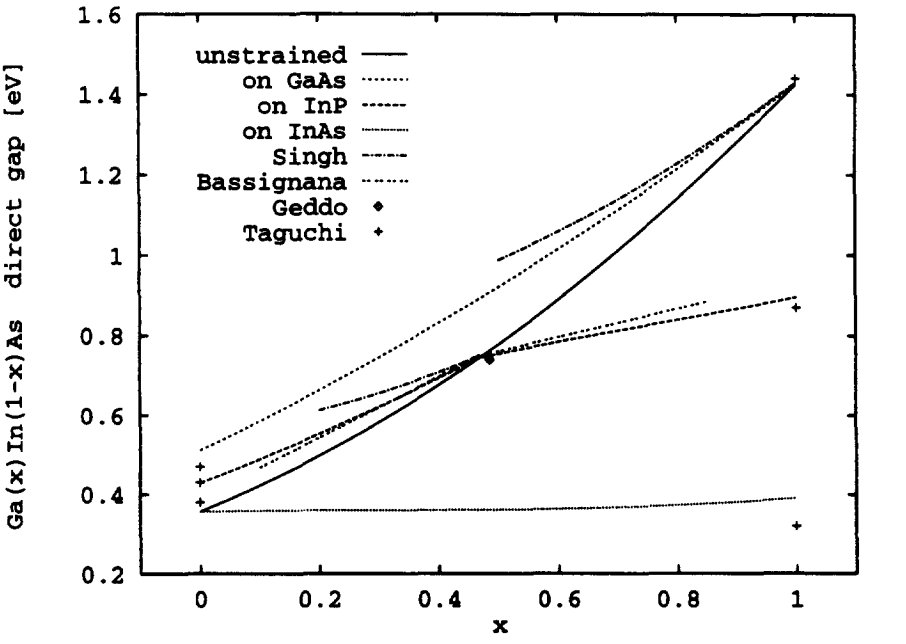


Fig. 7. Direct gap $E^{\Gamma}(x)$ for unstrained and coherently strained $Ga_xIn_{1-x}As$ on GaAs, InP, and InAs (001) substrate vs composition at 300 K.

Table 6. Coefficients for strain shift of parallel, perpendicular and DOS mass of $Ga_xIn_{1-x}As$ for (001) interface orientation

| | $\Delta m^\Gamma$ | | | $\Delta m^\Gamma_\perp$ | | | $\Delta m^\Gamma_d$ | | |
|---|---|---|---|---|---|---|---|---|---|
| | $x^0$ | $x^1$ | $x^2$ | $x^0$ | $x^1$ | $x^2$ | $x^0$ | $x^1$ | $x^2$ |
| $e^1$ | −0.319 | 0.132 | −0.147 | −0.33 | −0.168 | 0.104 | −0.321 | 0.0235 | −0.041 |
| $e^2$ | −3.65 | 11.21 | −7.60 | −2.10 | −0.593 | 1.692 | −3.051 | 5.932 | −3.128 |
| $e^3$ | −10.50 | 164.0 | −67.85 | −25.86 | −57.81 | 61.56 | −12.95 | 74.47 | −27.98 |

changes in $\Delta E_v$ by $\approx 0.5$ eV for a bond length change of 0.06 Å. Their calculations are supported by the recent experimental studies of Ohler *et al.*[46]. Since the bond lengths at the interface are functions of growth conditions, it seems to be this very influence that forbids to predict band offsets to an arbitrary degree of accuracy. Another influence is the inferior microscopic interface quality through additional defects (dangling bonds). Therefore, one should be aware of the rather high uncertainties when using band discontinuities calculated as band edge differences on an absolute scale.

## 5. EFFECTIVE ELECTRON MASS

The effective electron mass can be closely related to fundamental band parameters via $\mathbf{k}\cdot\mathbf{p}$ theory[47]. For the unstrained direct $\Gamma$ valley holds;

$$\frac{1}{m^\Gamma} = 1 + \frac{E_p}{3}\left(\frac{2}{E^\Gamma} + \frac{1}{E^\Gamma + \Delta_0}\right). \tag{24}$$

$E_p$ denotes the squared conduction ($\Gamma$) to valence band momentum matrix element. Terms resulting from higher bands can be neglected for III–V compounds since their gaps are much larger and the matrix elements are small. Linear interpolation of $E_p$ results in too small values at intermediate compositions, so we include bowing $C_{E_p} = 2.0$ eV[48]. Equation (24) then resembles measured values very well. The polynomial approximation of (24) for $Ga_xIn_{1-x}As$ at low temperature;

$$m^\Gamma(x, 0) = 0.0237 + 0.031x + 0.0122x^2, \tag{25}$$

shows a small deviation of $m^\Gamma$ from linearity. The effects of temperature can be calculated using (11). The dependence on $T$ is rather weak, so an Ansatz with a linear material independent temperature coefficient is sufficient;

$$m^\Gamma(x, T) = m^\Gamma(x, 0) - 1.2\cdot 10^{-5}\frac{T}{K}. \tag{26}$$

### 5.1. Strain effects

In the strained case $m^\Gamma$ becomes anisotropic. An extension of (24) leads to different masses parallel and perpendicular to the interface[49];

$$\frac{1}{m^\Gamma_\perp} = 1 + \frac{E_p}{3}\left(\frac{3}{2E^{\Gamma-hh}} + \frac{1}{2E^{\Gamma-lh}} + \frac{1}{E^{\Gamma-so}} + \frac{2\delta E}{\Delta_0}\left(\frac{1}{E^{\Gamma-lh}} - \frac{1}{E^{\Gamma-so}}\right)\right) \tag{27}$$

$$\frac{1}{m^\Gamma_\parallel} = 1 + \frac{E_p}{3}\left(\frac{2}{E^{\Gamma-lh}} + \frac{1}{E^{\Gamma-so}} - \frac{4\delta E}{\Delta_0}\left(\frac{1}{E^{\Gamma-lh}} - \frac{1}{E^{\Gamma-so}}\right)\right),$$

where $E^{\Gamma-hh}$ is the difference $E^\Gamma - E^{hh}$ under strain. The meaning of the differences $E^{\Gamma-lh}$, $E^{\Gamma-so}$ is analogous.

The strained mass parameters can be written as;

$$m^\Gamma_\parallel = m^\Gamma + \Delta m^\Gamma_\parallel \quad m^\Gamma_\perp = m^\Gamma + \Delta m^\Gamma_\perp, \tag{28}$$

where $\Delta m^\Gamma$ is approximated similar to (22). A cubic strain dependence with parabolic composition dependence gives a maximum relative error below 2% in the useful strain range of the GaInAs system. The density-of-states (DOS) mass can be expressed in the same way;

$$m^\Gamma_d = ((m^\Gamma_\parallel)^2 m^\Gamma_\perp)^{1/3} = m^\Gamma + \Delta m^\Gamma_d. \tag{29}$$

The coefficients are summarized in Table 6. Figure 8 shows a comparison of the fitted and $\mathbf{k}\cdot\mathbf{p}$ calculated parallel and perpendicular masses as well as the DOS mass. Our model is compared with the results of Jaffe and Singh[32], who included strain in their tight-binding band structure calculations, for GaInAs strained to GaAs in Fig. 9. Strain effects on the masses of the higher indirect gaps are usually neglected, since anisotropy caused by valley splitting is much more pronounced.

## 6. ELECTRON MOBILITY

Mobility in GaInAs on GaAs was studied theoretically by Kuhn and Darling[50] in the relaxation time approximation (RTA). Thobel *et al.*[51] investigated GaInAs coherently strained to GaAs and InP using the Monte Carlo (MC) technique. We also employ the MC technique to systematically study composition and strain effects causing the anisotropic behavior of $\mu_0$, since it removes the restrictions of the RTA and yields a self consistent distribution function. Our simulation

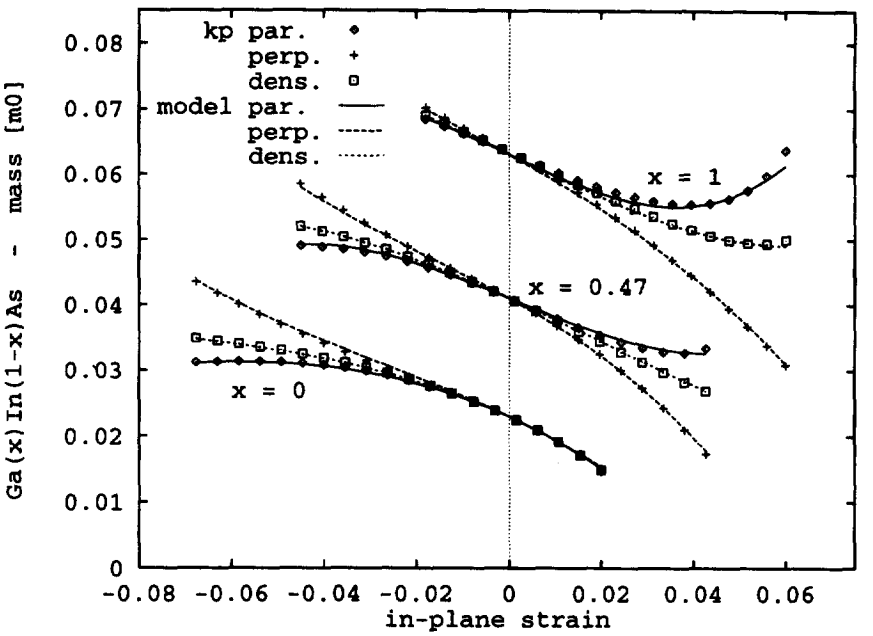


Fig. 8. **k·p** calculated (points) and fitted $m_{\parallel}^{\Gamma}$, $m_{\perp}^{\Gamma}$, and $m_{d}^{\Gamma}$ for $Ga_xIn_{1-x}As$ vs $e_{\parallel}$.

program incorporates a many-valley anisotropic nonparabolic band structure representation ($\Gamma$, $L$, $X$ valleys) and takes into account scattering by polar and nonpolar optical phonons, acoustic phonons, ionized impurities, and alloy disorder. Though full-band MC calculations give more exact results especially at strong non-equilibrium[52], the analytic band model allows to study material grading and strain effects in a straightforward manner. Table 7 shows the material parameters used in the MC calculation. The intervalley scattering parameters are taken from [53].

Figure 10 shows the calculated low-field mobility as a function of the composition $x$ for unstrained $Ga_xIn_{1-x}As$. A nonlinear regression gives;

$$\mu_0(x) = 30682 - 71341x + 88556x^2 - 57327x^3 + 17311x^4. \quad (30)$$

Figures 11 and 12 show the MC calculated mobilities $\mu_{\parallel}$ and $\mu_{\perp}$ parallel and perpendicular to the interface,

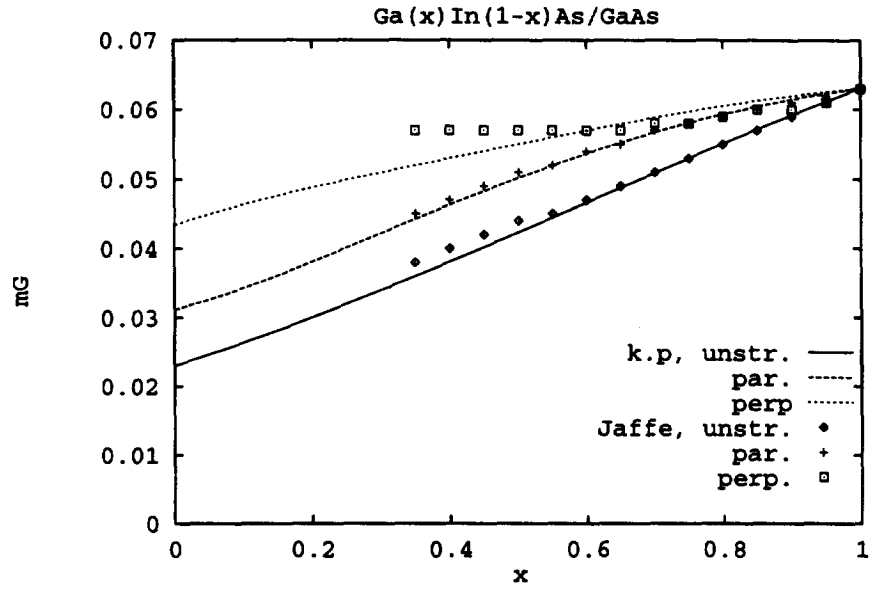


Fig. 9. $m_{\parallel}^{\Gamma}$ and $m_{\perp}^{\Gamma}$ for $Ga_xIn_{1-x}As$ strained to GaAs and unstrained $m^{\Gamma}$ vs $x$ compared to Ref. [32].

Table 7. Material parameters used in MC calculation

| Quantity | | GaAs | | | InAs | | | Unit |
|---|---|---|---|---|---|---|---|---|
| $v_l$ | | 5.23 | | | 4.28 | | | $10^5$ cm s$^{-1}$ |
| $v_t$ | | 2.47 | | | 2.65 | | | $10^5$ cm s$^{-1}$ |
| $\epsilon_s$ | | 12.9 | | | 15.15 | | | $\epsilon_0$ |
| $\epsilon_\infty$ | | 10.92 | | | 12.75 | | | $\epsilon_0$ |
| | | 5.36 | | | 5.67 | | | g cm$^{-3}$ |
| $\hbar\omega_{LO}$ | | 36.25 | | | 30.2 | | | meV |
| | | $\Gamma$ | $L$ | $X$ | $\Gamma$ | $L$ | $X$ | |
| $\alpha$ | | 0.61 | 0.461 | 0.204 | 1.39 | 0.536 | 0.90 | eV$^{-1}$ |
| $D_{ac}$ | | 7.0 | 9.2 | 9.27 | 8.0 | 8.0 | 8.0 | eV |
| $D_0$ | | — | 3.0 | — | — | 3.0 | — | $10^8$ eV cm$^{-1}$ |
| $D_{iv}$ | $\Gamma$ | — | 10.0 | 10.0 | — | 10.0 | 10.0 | $10^8$ eV cm$^{-1}$ |
| | $L$ | 10.0 | 10.0 | 5.0 | 10.0 | 10.0 | 9.0 | $10^8$ eV cm$^{-1}$ |
| | $X$ | 10.0 | 5.0 | 7.0 | 10.0 | 9.0 | 9.0 | $10^8$ eV cm$^{-1}$ |
| $\hbar\omega_{iv}$ | $\Gamma$ | — | 27.8 | 29.9 | — | 27.8 | 29.9 | meV |
| | $L$ | 27.8 | 29.0 | 29.3 | 27.8 | 29.0 | 29.3 | meV |
| | $X$ | 29.9 | 29.3 | 29.9 | 29.9 | 29.3 | 29.9 | meV |
| $D_{all}$ | | | | 0.5 | | | | eV |

respectively. Compressive strain degrades while tensile strain enhances both values. However, for Ga-rich alloys at very large positive strain, a slightly nonmonotonic behavior is observed in $\mu$ which is caused by an increase of $m_\parallel$ for $e_\parallel > 4\%$ (Fig. 8). Anisotropy is significant for $e_\parallel > 1\%$. Since we study bulk transport, the effects of dislocations which can reduce the mobility significantly are neglected, so the results must be considered as an upper limit in the case of partially relaxed layers.

First it is observed that;

$$\frac{\mu}{\mu_\perp} = \frac{m_\perp}{m_\parallel}, \tag{31}$$

as one expects from a first-order perturbation calculation of the Boltzmann transport equation (BTE) for an ellipsoidal valley and isotropic relaxation rate. Second, if we define an average mobility;

$$\mu_{av} = (\mu_\perp \mu^2)^{1/3}, \tag{32}$$

we find that it scales as;

$$\mu_{av} = \mu_0 \left(\frac{m_0}{m_d}\right)^\eta, \tag{33}$$

where $\eta$ only weakly deviates from 3/2 over the whole composition range. This behavior is surprising since the dominant scattering process governing mobility, polar optical phonon scattering, is both anisotropic and inelastic, and thus no relaxation time can be

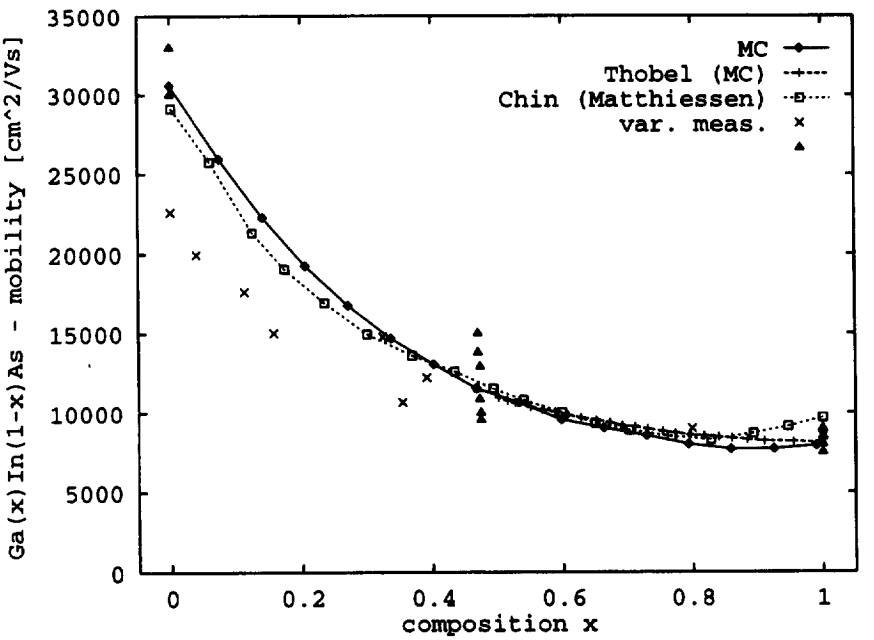


Fig. 10. Low-field mobility of unstrained $Ga_xIn_{1-x}As$ at 300 K.

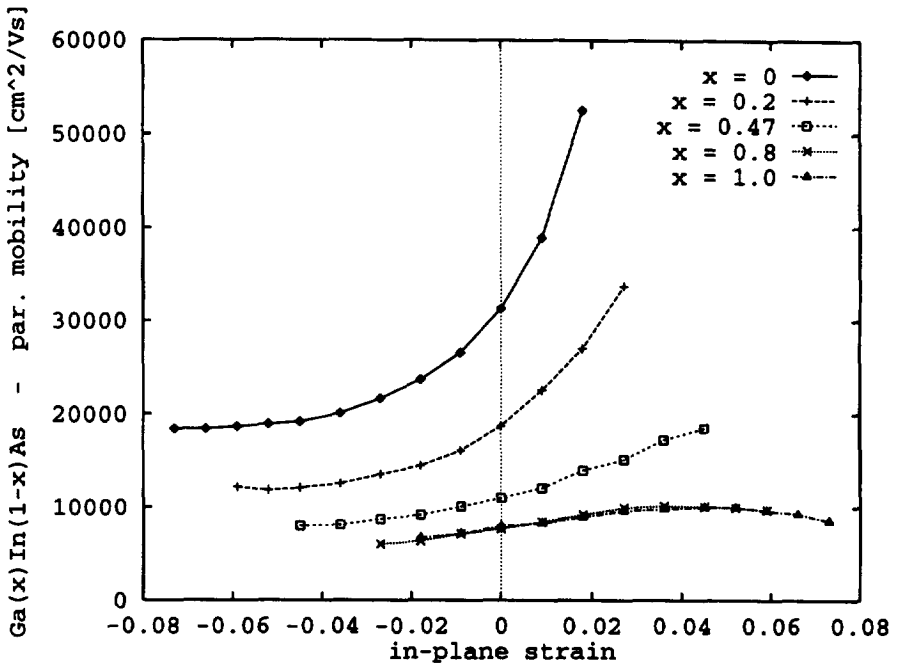


Fig. 11. MC calculated low-field mobility at 300 K parallel to (001) interface vs $e_{\parallel}$.

defined strictly. The present results, however, justify the assumption of an approximate relaxation time with mass exponent $-1/2$ according to the BTE solution[54].

This behavior allows a model to be constructed which relates the strained mobilities to the unstrained virtually by use of the model for the strained masses ((28) and (29));

$$\mu_{\parallel} = \mu_0 \frac{m_0^{\eta}}{m_{\parallel} m_d^{\eta-1}} = \frac{\mu_0}{\left(1 + \frac{\Delta m_{\parallel}}{m_0}\right)\left(1 + \frac{\Delta m_d}{m_0}\right)^{\eta-1}} \tag{34}$$

$$\mu_{\perp} = \mu_0 \frac{m_0^{\eta}}{m_{\perp} m_d^{\eta-1}} = \frac{\mu_0}{\left(1 + \frac{\Delta m_{\perp}}{m_0}\right)\left(1 + \frac{\Delta m_d}{m_0}\right)^{\eta-1}}. \tag{35}$$

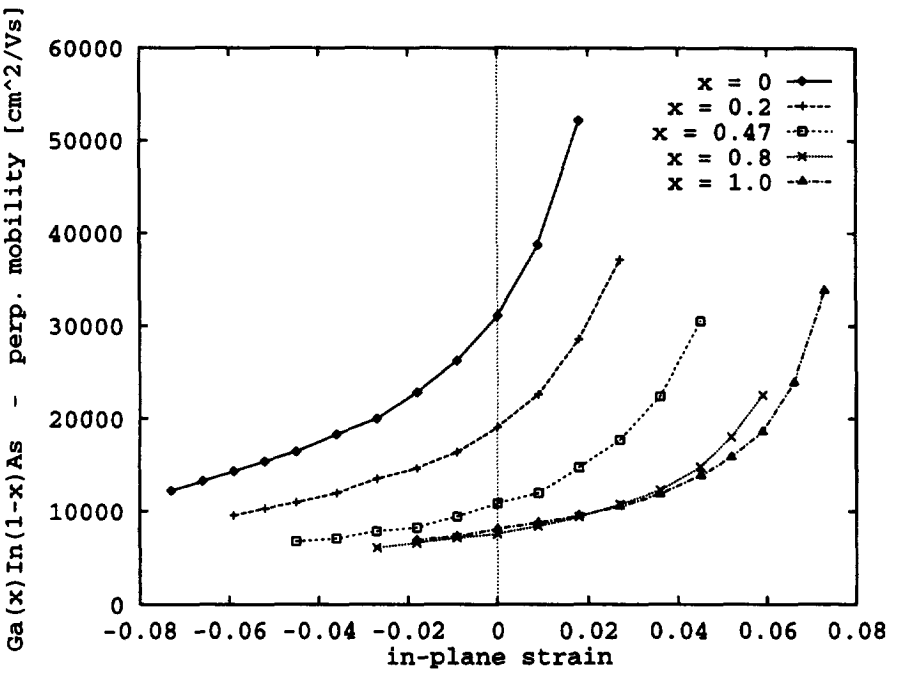


Fig. 12. MC calculated low-field mobility at 300 K perpendicular to (001) interface vs $e_{\parallel}$.

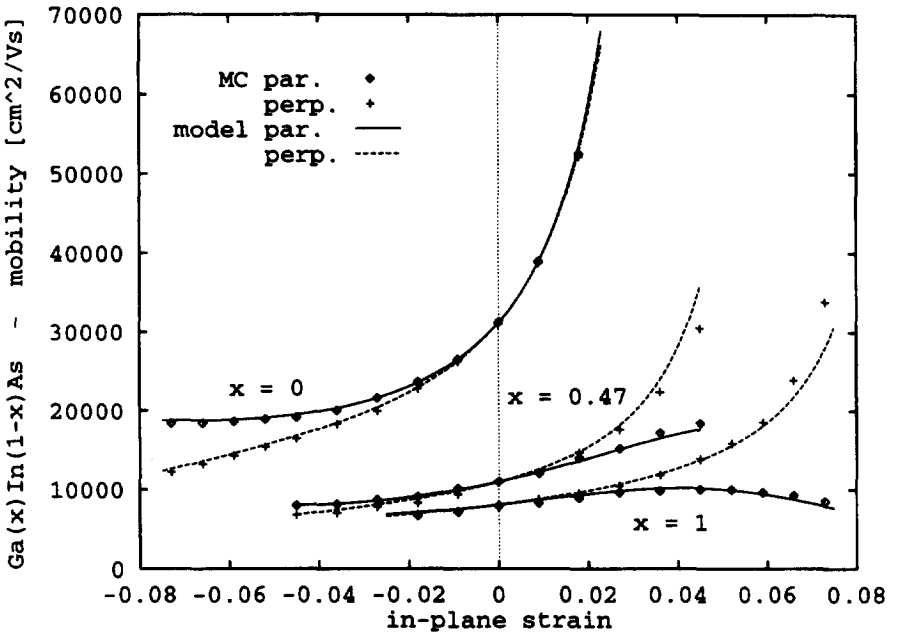


Fig. 13. Low-field mobility versus $e_{\parallel}$ at 300 K obtained from the strain model compared to MC data.

Figure 13 shows a comparison of the constructed model with the MC data. The correspondence is good, at low Ga content and/or low strain it is excellent.

## 7. CONCLUSION

Based on models for the strain dependent shifts of the band edges and changes of the effective mass which were obtained from deformation potential and $\mathbf{k}\cdot\mathbf{p}$ theory, we have investigated the effects of strain on the low-field mobility of GaInAs alloys. An analytical model for the anisotropic mobility has been constructed which resembles the MC calculated values very well. For the whole strain range in the GaAs-InAs system all models were formulated as functions of the independent parameters composition and in-plane strain, which are no longer proportional for partially relaxed layers. Additionally, empirical estimations for the critical thickness for dislocation free growth and residual strain for relaxed layers are given which take into account growth and annealing temperature.

*Acknowledgement*—This work is supported by the laboratories of SIEMENS AG at Munich, Germany.

## REFERENCES

1. Kosina, H., Harrer, M., Vogl, P. and Selberherr, S., in *Simulation of Semiconductor Devices and Processes*, ed. H. Ryssel and P. Pichler, Springer, 1995, Vol. 6, pp. 396–399.
2. van Vechten J. and Bergstresser, T., *Phys. Rev. B.* 1970, **1**, 3351.
3. Adachi, S., *J. Appl. Phys.*, 1987, **61**, 4869.
4. Hinckley, J. and Singh, J., *J. Appl. Phys.*, 1991, **69**, 2694.
5. Hinckley, J. and Singh, J., *Phys. Rev. B.*, 1990, **42**, 3546.
6. Matthews, J. and Blakeslee, A., *J. Cryst. Growth.*, 1974, **27**, 118.
7. Matthews, J. and Blakeslee, A., *J. Cryst. Growth.*, 1975, **29**, 273.
8. Matthews, J. and Blakeslee, A., *J. Cryst. Growth.*, 1976, **32**, 265.
9. Downes, J., Dunstan, D. and Faux, D., *Semicond. Sci. Technol.*, 1994, **9**, 1265.
10. van der Merwe, J., *J. Electron. Mater.*, 1991, **20**, 793.
11. Fitzgerald, E., in Ref. [72], Section 1.2, pp. 6–15.
12. Krishnamoorthy, V., *et al.*, *Appl. Phys. Lett.*, 1992, **61**, 2680.
13. Dunstan, D., Kidd, P., Howard, L. and Dixon, R., *Appl. Phys. Lett.*, 1991, **59**, 3390.
14. Maigné, P. and Baribeau, J.-M., *J. Appl. Phys.*, 1994, **76**, 1962.
15. Lourenço, M., Homewood, K. and Considine, L., *Mat. Sci. Eng. B*, 1994, **28**, 507.
16. Zou, J., Usher, B., Cockayne, D. and Glaisher, R., *J. Electron. Mater.*, 1991, **20**, 855.
17. People, R. and Bean, J., *Appl. Phys. Lett.*, 1985, **47**, 322.
18. People, R. and Bean, J., *Appl. Phys. Lett.*, 1986, **49**, 229.
19. Kui, J. and Jesser, W., *J. Electron. Mater.*, 1991, **20**, 827.
20. Varshni, Y., *Physica*, 1967, **34**, 149.
21. Brooks, H., in *Advances in Electronics and Electron Physics*, ed. L. Marton, Academic Press, 1955, Vol. 8.
22. Herring, C. and Vogt, E., *Phys. Rev.*, 1956, **101**, 833.
23. Kane, E., *Phys. Rev.*, 1970, **178**, 1368.
24. Kleiner, W. and Roth, L., *Phys. Rev. Lett.*, 1959, **2**, 334.
25. Pollak, F. and Cardona, M., *Phys. Rev.*, 1968, **172**, 816.
26. Bir, G. and Pikus, G., *Symmetry and Strain-Induced Effects in Semiconductors*, Wiley, 1974, p. 300.
27. Cardona, M. and Christensen, N., *Phys. Rev. B*, 1987, **35**, 6182.
28. Van de Walle, C., *Phys. Rev. B*, 1989, **39**, 1871.

29. Geddo, M., Bellani, V. and Guizzetti, G., *Phys. Rev. B*, 1994, **50,** 5456.
30. Kuo, C., Vong, S., Cohen, R. and Stringfellow, G., *J. Appl. Phys.*, 1985, **57,** 5428.
31. Bassignana, I., Miner, C. and Puetz, N., *J. Appl. Phys.*, 1989, **65,** 4299.
32. Jaffe, M. and Singh, J., *J. Appl. Phys.*, 1989, **65,** 329.
33. Singh, J., in Ref. [72], Section 3.1, pp. 61–69.
34. Bimberg, D. and Srocka, B., in Ref. [72], Section 6.1, pp. 159–168.
35. Taguchi, A. and Ohno, T., *Phys. Rev. B*, 1989, **39,** 7803.
36. Paul, S., Roy, J. and Basu, P., *J. Appl. Phys.*, 1991, **69,** 827.
37. Anderson, R., *Solid-St. Electron.*, 1962, **5,** 341.
38. Harrison, W., *J. Vac. Sci. Technol.*, 1977, **14,** 1016.
39. Harrison, W., *J. Vac. Sci. Technol. B*, 1985, **3,** 1231.
40. Van Vechten, J., *J. Vac. Sci. Technol. B.*, 1985, **3,** 1240.
41. Tersoff, J., *Phys. Rev. B.*, 1984, **30,** 4874.
42. Van de Walle, C. and Martin, R., *Phys. Rev. B*, 1987, **35,** 8154.
43. Margaritondo, G. and Perfetti, P., in *Heterojunction Band Discontinuities*, ed. F. Capasso and G. Margaritondo, Elsevier, 1987, Ch. 2, pp. 59–114.
44. Yu, E., McCaldin, J. and McGill, T., in *Solid State Physics*, ed. H. Ehrenreich and D. Turnbull, Academic Press, 1992, Vol. 46, pp. 1–146.
45. Oloumi, M. and Matthai, C., *J. Phys.: Condensed Matter*, 1990, **2,** 5153.
46. Ohler, C., Kohleick, R., Förster, A. and Lüth, H., *Phys. Rev. B*, 1994, **50,** 7833.
47. Hermann, C. and Weisbuch. C., *Phys. Rev. B*, 1977, **15,** 823.
48. Berolo, O., Woolley, J. and Van Vechten, J., *Phys. Rev. B*, 1973, **8,** 3794.
49. Hendorfer, G. and Schneider, J., *Semicond. Sci. Technol.*, 1991, **6,** 595.
50. Kuhn, K. and Darling, R., *IEEE Trans. Electron. Devices*, 1992, **39,** 1288.
51. Thobel, J., *et al.*, *Appl. Phys. Lett.*, 1990, **56,** 346.
52. Fischetti, M., *IEEE Trans. Electron Devices*, 1991, **38,** 634.
53. Brennan, K. and Hess, K., *Solid-St. Electron.*, 1984, **27,** 347.
54. Conwell, E., *High Field Transport in Semiconductors*, Vol. 9 of *Solid State Physics*, Academic Press, 1967, p. 197.
55. Chin, V. and Tansley, T., *Solid-St. Electron.*, 1991, **34,** 1055.
56. Blakemore, J., *J. Appl. Phys.*, 1982, **53,** R123.
57. Adachi, S., *J. Appl. Phys.*, 1982, **53,** 8775.
58. Aspnes, D., *Phys. Rev. B.*, 1976, **14,** 5331.
59. Wang, P., *et al.*, *Semicond. Sci. Technol.*, 1992, **7,** 767.
60. Wilkinson, V. and Adams, A., in Ref. [72], Section 3.2, pp. 70–75.
61. Pollak, F., in *Properties of Aluminium Gallium Arsenide*, No. 7 in *EMIS Datareviews Series*, ed S. Adachi (IEE INSPEC, 1993), Section 4.1, pp. 53–57.
62. Krijn, M., *Semicond. Sci. Technol.*, 1991, **6,** 27.
63. Nahory, R., Pollack, M., Johnston, W. and Barns, R., *Appl. Phys. Lett.*, 1978, **33,** 659.
64. Bouarissa, N. and Aourag, H., *Mat. Sci. Eng. B*, 1995, **33,** 122.
65. Landolt, M. and Börnstein, J, *Numerical Data and Functional Relationships in Science and Technology*, Vol. 22/A of *New Series, Group III*, Springer, 1987.
66. Giesecke, G., in *Physics of III–V Compounds*, Vol. 2 of *Semiconductors and Semimetals*, ed. R. Willardson and A. Beer, Academic Press, 1966, Ch. 4.
67. Singh, J., *Physics of Semiconductors and their Heterostructures*, McGraw–Hill, 1993, p. 151.
68. Adachi, S., *J. Appl. Phys.*, 1985, **58,** R1.
69. Nolte, D., Walukiewicz, W. and Haller, E. *Phys. Rev. Lett.*, 1987, **59,** 501.
70. Adachi, S., *Physical Properties of III–V Semiconductor Compounds*, Wiley, 1992, p. 118.
71. *Properties of Lattice-Matched and Strained Indium Gallium Arsenide*, No. 8 in *EMIS Datareviews Series*, ed. P. Bhattacharya, IEE INSPEC, 1993.